catalysts

MDPI

Article

A Pd/MnO_2 Electrocatalyst for Nitrogen Reduction to Ammonia under Ambient Conditions

Chang Sun, Yingxin Mu and Yuxin Wang *

State Key Laboratory of Chemical Engineering, School of Chemical Engineering, Tianjin University, Tianjin 300350, China; sunchangtju@163.com (C.S.); muyingxin@tju.edu.cn (Y.M.)

* Correspondence: yxwang@tju.edu.cn; Tel.: +86-22-2789-0515

Received: 22 June 2020; Accepted: 17 July 2020; Published: 19 July 2020

Abstract: Electrochemical ammonia synthesis, which is an alternative approach to the Haber–Bosch process, has attracted the attention of researchers because of its advantages including mild working conditions, environmental protection, and simple process. However, the biggest problem in this field is the lack of high-performance catalysts. Here, we report high-efficiency electroreduction of N_2 to NH_3 on γ-MnO_2-supported Pd nanoparticles (Pd/γ-MnO_2) under ambient conditions, which exhibits excellent catalytic activity with an NH_3 yield rate of 19.72 μg·mg^{-1}_{Pd} h^{-1} and a Faradaic efficiency of 8.4% at −0.05 V vs. the reversible hydrogen electrode (RHE). X-ray diffraction (XRD) and transmission electron microscopy (TEM) characterization shows that Pd nanoparticles are homogeneously dispersed on the γ-MnO_2. Pd/γ-MnO_2 outperforms other catalysts including Pd/C and γ-MnO_2 because of its synergistic catalytic effect between Pd and Mn.

Keywords: electrochemical synthesis of ammonia; palladium; ambient conditions; MnO_2; synergistic catalytic

1. Introduction

Nitrogen is the most abundant gas in the atmosphere. The product of nitrogen fixation, especially ammonia (NH_3), not only is vital to life but also plays a key role in many other fields, such as transportation, refrigerants, and fertilizer. More than 80% of ammonia is used to manufacture chemical fertilizer [1]. Besides, ammonia is not only an important inorganic chemical product but also a key fuel and energy storage material. The flammability range is narrow, so it is easier to store and transport than liquid hydrogen [2,3]. The main way of nitrogen fixation in the industry is the Haber–Bosch process, which converts N_2 and H_2 into ammonia on Fe-based catalysts. However, the Haber–Bosch process needs harsh conditions, and the required energy comes from coal and natural gas, leading to its energy consumption occupies the world's energy supply more than 1% every year. Moreover, this process produces more than 300 million tons of CO_2 each year [4–6]. So it is necessary to develop new methods of ammonia synthesis which can avoid these drawbacks [7–11].

One promising approach to the Haber−Bosch process is to use electrical energy to drive the ammonia synthesis reaction [12–14]. This approach of ammonia synthesis has numerous advantages including low working temperature, low working pressure, environmental protection, and simple process, especially as the emission of CO_2 in this process is much lower than that in the Haber–Bosch process [15]. So electrochemical synthesis of ammonia has attracted the attention of researchers in recent years. At present, many electrocatalysts have been proved that have effective catalytic performance. Precious metal catalysts are the earliest reported batches of electrochemical ammonia synthesis catalysts, including Pt, Ir, Pd, Au, etc. The NH_3 yield rate of most precious metal catalysts is between 9×10^{-11} mol/(s·cm^2) and 10^{-12} mol/(s·cm^2) [16–22]. Lan et al. studied the electrochemical synthesis of ammonia with water and air using Pt/C as the catalyst [23,24]. The maximum NH_3 yield rate

can reach 3.50×10^{-9} mol/(s·cm^2). However, the Faradaic efficiency of Ir and Pt catalysts are extremely low because they are effective hydrogen evolution reaction (HER) catalysts. Many non-precious metal catalysts also exhibit effective catalytic performance. Fe is the most widely used catalyst for nitrogen fixation in the industry. Recently, inspired by natural nitrogen fixation, more Mo catalysts have also been reported [25–27]. Besides, more transition metals, including Mn and Ti, have also been reported for electrocatalytic reduction of dinitrogen to NH_3 [28,29]. However, most of the electrocatalysts have low activity and Faradaic efficiency for NH_3 production. Therefore, the improvement of electrocatalysts is essential for the progress of electrochemical ammonia synthesis, which needs a better design of N_2 reduction reaction (NRR) electrocatalyst and the electrochemical system [17,24,30–38]. Liu et al. reported an effective biomimetic strategy to boost electrocatalytic N_2 fixation, which shows that the effective design of the electrochemical system is important for the progress of electrochemical ammonia synthesis [39].

There are two major steps in the process of electrocatalytic synthesis of ammonia: N_2 adsorption on electrocatalyst and hydrogenation of nitrogen molecules on the surface of the electrocatalyst. Mukundan et al. demonstrated this process by using origami-like Mo_2C as the catalyst of electrochemical ammonia synthesis [40]. However, almost no electrocatalyst performs well in both steps. Skulason [41] proposed through simulation calculations that when the adsorption energy of N atoms on the surface of electrocatalyst is bigger than that of H atoms, N atoms cover most of the surface of the catalyst to improve NRR selectivity while suppressing hydrogen evolution reaction (HER). Studies [42,43] have shown that Mn, Re, and other pre-transition metal elements have strong adsorption energy for N_2 molecules. But these elements are usually inefficient in the hydrogenation of N_2 molecules, which is another major step in the electrocatalytic synthesis of ammonia. However, Pd, Ni, and other post-transition metal elements perform well in hydrogenation reactions, but have low adsorption energy of N_2. Especially for Pd, it is easy to absorb hydrogen atoms in its lattice to form PdH, and can achieve hydrogenation reaction easier than other metal catalysts through the Grotthuss-like proton-hopping mechanism [21,44–46]. Consequently, combining multiple catalysts with different advantages in the ammonia synthesis process is a promising design for NRR electrocatalyst.

In this study, we effectively load Pd nanoparticles on the surface of Mn by the polyol reduction method and report high-performance electroreduction N_2 to NH_3 on Pd/γ-MnO_2 under ambient conditions, which exhibits high activity and selectivity with an NH_3 yield rate of 19.72 μg·mg^{-1} $_{Pd}$ h^{-1} (6.44×10^{-11} mol·s^{-1} cm^{-2}) and a Faradaic efficiency of 8.4% at −0.05 V vs. the reversible hydrogen electrode (RHE). The result shows that γ-MnO_2 is the best carrier of Pd among the three crystal forms of MnO_2. The performance of Pd/γ-MnO_2 demonstrates the synergistic catalytic effect between Pd and Mn, which is an promising design strategy for NRR catalysts.

2. Results and Discussion

2.1. Characterization of Catalyst

The MnO_2 were prepared by the hydrothermal method and the preparation method of Pd/γ-MnO_2 and Pd/C catalysts was polyol reduction method. Scanning electron microscope (SEM) image and X-ray diffraction (XRD) pattern of γ-MnO_2 were shown in Figure 1. γ-MnO_2 has a flower-like structure, suggesting that it's a suitable carrier for metal particles. The peaks in Figure 1b with 2θ values of 22.1°, 37.1°, 42.2°, 55.8°, and 67.8° can be indexed to the diffraction from (101), (210), (211), (212), and (511) lattice planes of γ-MnO_2 (JCPDS #44-0142).

As shown in Figure 2a, the Pd nanoparticles are loaded on the surface of carbon black XC-72. Figure 2b is the transmission electron microscopy (TEM) images of γ-MnO_2 without Pd particles on it. Figure 3 shows TEM and energy dispersive x-ray spectroscopy (EDX) mapping images of the obtained Pd/γ-MnO_2 catalysts, which suggest that the Pd nanoparticles are more evenly dispersed on γ-MnO_2 than those on the carbon black. Figure 3a,b show that Pd nanoparticle average sizes around 4 nm. Figure 3b shows the atomic lattice fringes of the Pd particles with lattice plane spacings determined to

be 0.225 nm, corresponding to the (111) lattice spacing of Pd. Figure 3c,d were EDX mapping images of Pd and Mn elements on Pd/γ-MnO_2, demonstrate that Pd can be detected throughout the surface of γ-MnO_2.

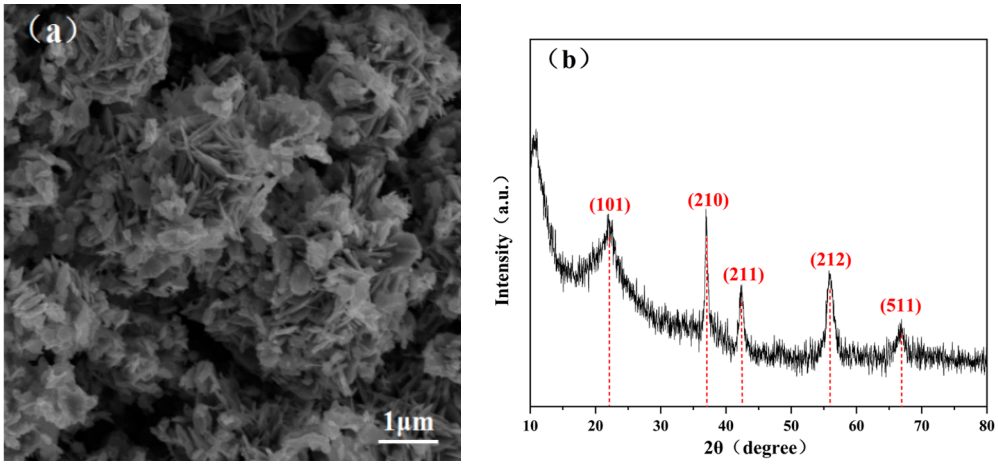

Figure 1. Scanning electron microscope (SEM) image (**a**) and X-ray diffraction (XRD) pattern (**b**) of γ-MnO_2.

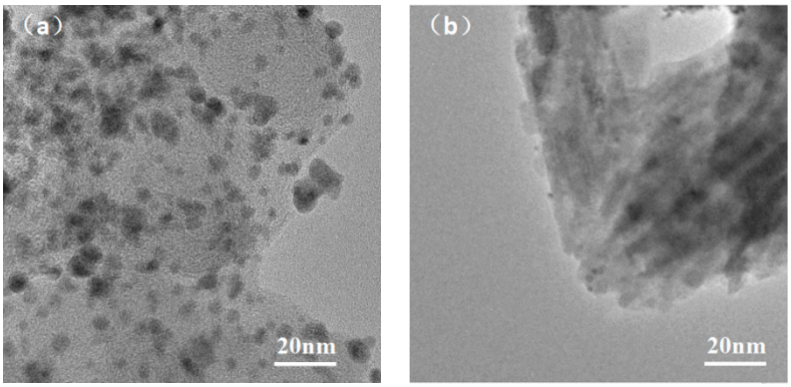

Figure 2. Transmission electron microscopy (TEM) images of (**a**) Pd/C and (**b**) γ-MnO_2.

Figure 4 shows the X-ray diffraction (XRD) pattern of the Pd/γ-MnO_2 catalyst. It was found that the diffraction peaks at 22.1°, 37.1°, 42.2°, and 55.8° correspond to (101), (210), (211), and (212) lattice planes of γ-MnO_2 (JCPDS #44-0142), and the peaks at 40.0°, 46.6°, and 68.1° correspond to (111), (200), and (220) lattice planes of Pd (JCPDS#65-2867). Figures 3 and 4 demonstrate that Pd nanoparticles were successfully dispersed on the surface of γ-MnO_2 by the polyol reduction method.

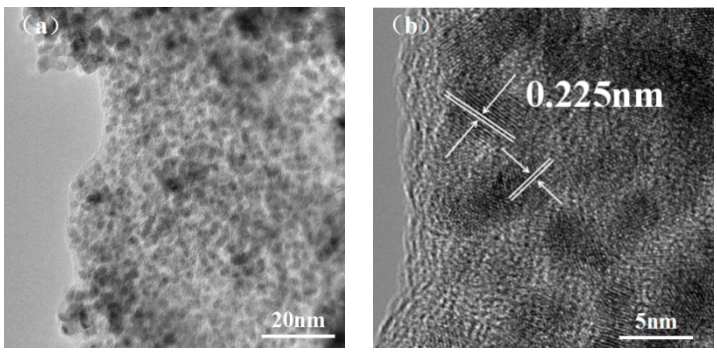

Figure 3. *Cont.*

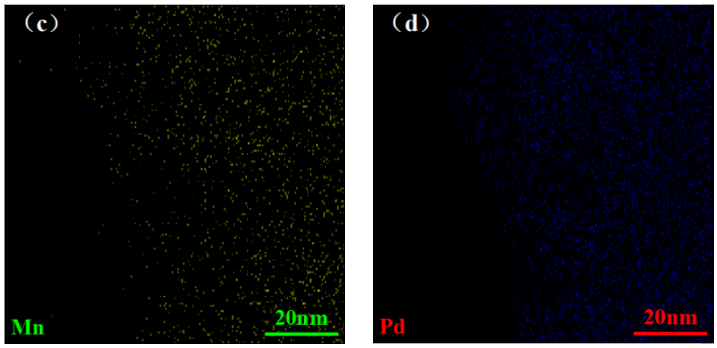

Figure 3. TEM images (**a**,**b**) of Pd/γ-MnO_2, and energy dispersive x-ray spectroscopy (EDX) mapping images (**c**,**d**) of Mn and Pd elements on Pd/γ-MnO_2.

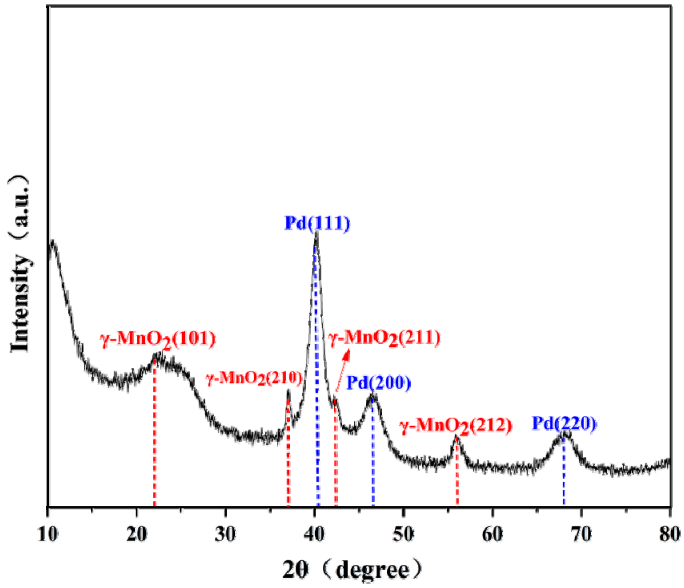

Figure 4. XRD pattern of Pd/γ-MnO_2 catalyst.

2.2. Electroreduction of N_2 to NH_3 on Pd/γ-MnO_2 Catalyst

The electrolysis experiments were performed using a gas-tight single compartment electrochemical cell which is filled with 0.1 M KOH as the electrolyte. A piece of Pt gauze and saturated calomel electrode were used as counter electrode and reference electrode, respectively. N_2 gas was delivered into the cell by N_2 gas bubbling. The NRR activities and Faradaic efficiencies of the electrodes were measured by controlled potential electrolysis with N_2-saturated electrolyte for 3 h. The NH_3 produced by electrode was quantified at the end of each electrolysis process using the calibration curves established by the indophenol blue method.

To illustrate whether Pd and Mn have a synergistic catalytic effect for electrochemical ammonia synthesis. We compared the catalytic performance of the Pd/γ-MnO_2 catalyst with Pd/C and γ-MnO_2 catalysts in three N_2-saturated electrolytes at −0.05 V vs. RHE. As is shown in Figure 5, the NH_3 yield rate and Faradaic efficiency on Pd/γ-MnO_2 catalyst are both higher than those on Pd/C and γ-MnO_2 catalysts. The NH_3 yield rate on Pd/γ-MnO_2 reaches 3.94 $\mu g \cdot mg^{-1}_{cat}\ h^{-1}$, which is around two times of that on Pd/C (2.11 $\mu g \cdot mg^{-1}_{cat}\ h^{-1}$) and around four times of that on γ-MnO_2 (1.17 $\mu g \cdot mg^{-1}_{cat}\ h^{-1}$). Considering the Pd loading is 20 wt.%, it can reach an NH_3 yield rate of 19.72 $\mu g \cdot mg^{-1}_{Pd}\ h^{-1}$ on Pd/γ-MnO_2.

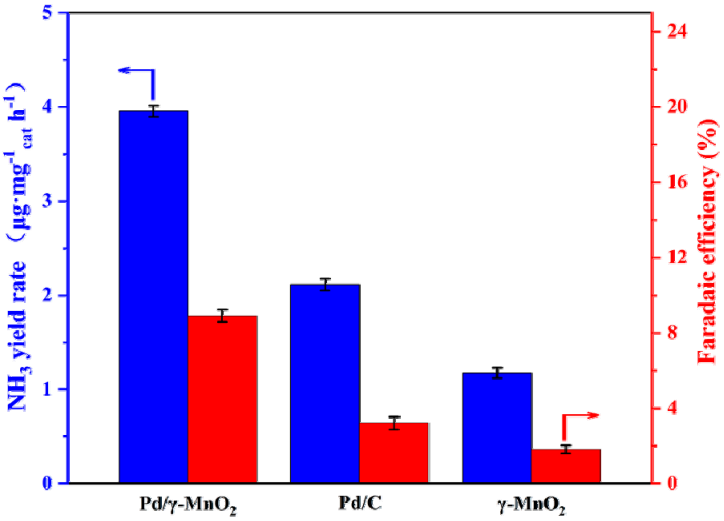

Figure 5. Comparison of the Pd/γ-MnO_2 catalyst with Pd/C and γ-MnO_2 catalysts for catalytic performance at -0.05 V in 0.1 M KOH.

Figure 6 shows that the NH_3 yield rates on Pd/γ-MnO_2 catalysts are invariably higher than those on the other two catalysts in a wide potential range, and reaches a maximum value at −0.05 V. The γ-MnO_2 catalyst shows a low NH_3 yield rate and Faradaic efficiency without Pd particles. However, γ-MnO_2-supported Pd nanoparticles outperform the Pd/C catalyst, indicating a synergistic catalytic effect for electroreduction of N_2 to NH_3 between Pd and Mn. The Pd/γ-MnO_2 catalysts combine different advantages of Pd and Mn. The reaction active site is at the phase interface of Pd and γ-MnO_2. To be specific, Mn adsorbs a large amount of N_2 at first because of its strong adsorption capacity for nitrogen molecules [29], and then Pd achieves hydrogenation for N_2 through its unique hydrogenation ability (Grotthuss-like proton-hopping mechanism) [21]. This synergy effect significantly accelerates the two major steps in the ammonia synthesis process. And Pd nanoparticles is evenly dispersed on the surface of γ-MnO_2, with a huge electrochemically active area, resulting in its unique catalytic activity. The Pd/γ-MnO_2 catalyst achieves an NH_3 yield rate and Faradaic efficiency that are comparable to the recently reported catalysts for NRR under ambient conditions. The less favorable kinetics of HER on Pd/γ-MnO_2 is because of its higher barrier for mass and charge transfer, as evidenced by the electrochemical impedance spectra (EIS) in Figure 7. The EIS image of Pd/γ-MnO_2 catalyst has a larger radius than Pd/C and γ-MnO_2, which indicates its larger barrier to HER. Therefore, the Pd/γ-MnO_2 catalyst has the highest NRR selectivity among the three.

In addition, we have investigated the NRR activity and Faradaic efficiency of Pd/α-MnO_2 and Pd/β-MnO_2 at −0.05 V. As shown in Figure 8, the Pd/γ-MnO_2 catalyst has superior NRR activity and selectivity than Pd/α-MnO_2 and Pd/β-MnO_2, indicating that γ-MnO_2 is the optimal carrier of Pd nanoparticles among these three crystal forms of MnO_2. This result is due to their different microstructures. As shown in Figure 9, the aggregation of Pd particles was easier to happen when we disperse Pd on α-MnO_2 and β-MnO_2. Pd particles can be more homogeneously dispersed on the surface of γ-MnO_2 than α-MnO_2 and β-MnO_2, and have a smaller particle size, which increases the catalyst surface area. The reactive sites of NRR possibly at the interface between the Pd and Mn. Therefore, the homogeneous dispersion of Pd nanoparticles provides more electrochemical reactive sites for NRR, while suppressing the competing HER. The aggregation of Pd particles on Pd/α-MnO_2 and Pd/β-MnO_2 leads to the more favorable kinetics of HER, as evidenced by the EIS image in Figure 10.

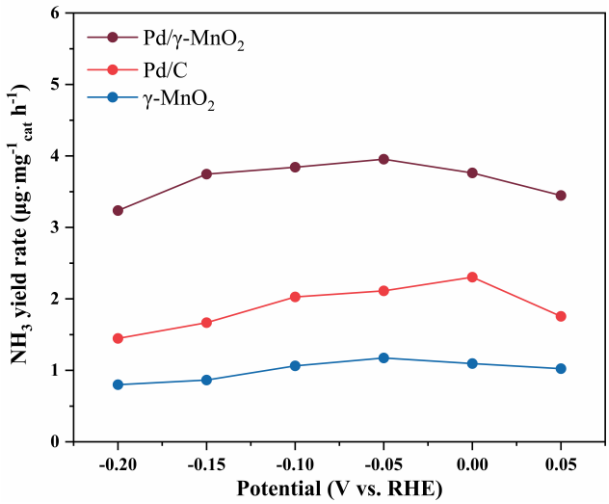

Figure 6. The NH_3 yield curves on Pd/γ-MnO_2, Pd/C, and γ-MnO_2 catalysts at various potentials.

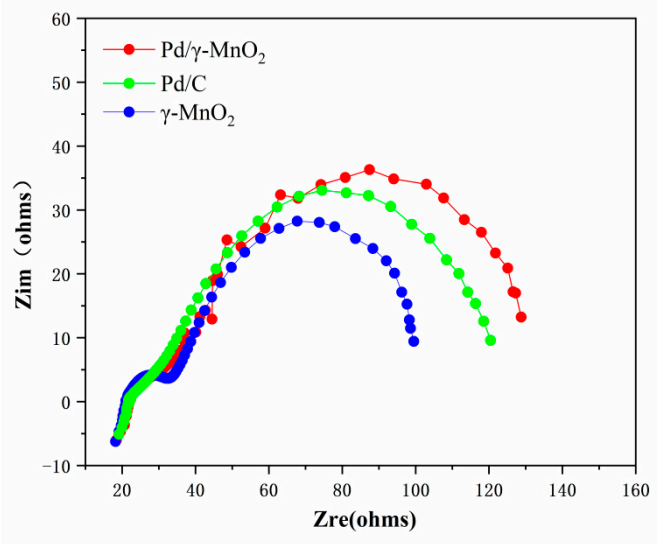

Figure 7. Electrochemical impedance spectra of Pd/γ-MnO_2, Pd/C, and γ-MnO_2 catalysts.

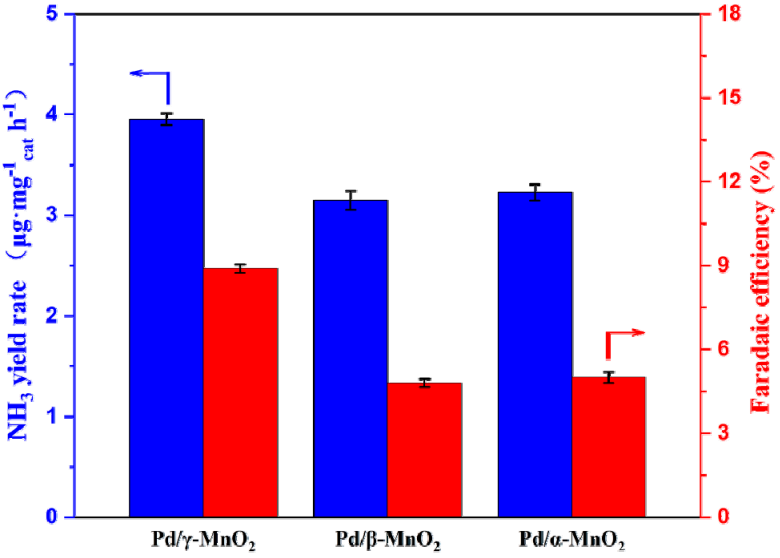

Figure 8. Comparison of the Pd/γ-MnO_2 catalyst with Pd/α-MnO_2 and Pd/β-MnO_2 catalysts for catalytic performance at −0.05 V in 0.1 M KOH.

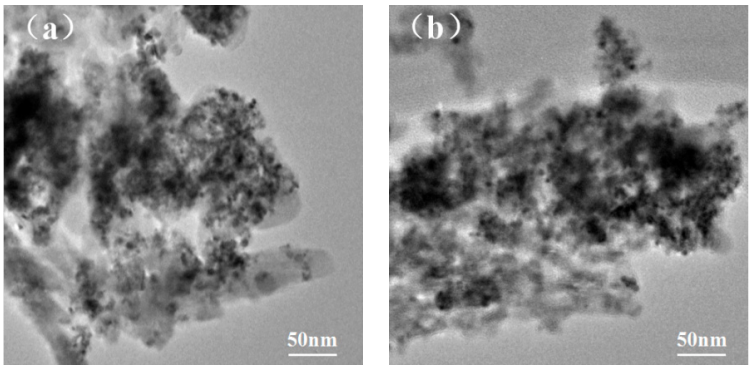

Figure 9. TEM images of (**a**) Pd/α-MnO_2 and (**b**) Pd/β-MnO_2 catalysts.

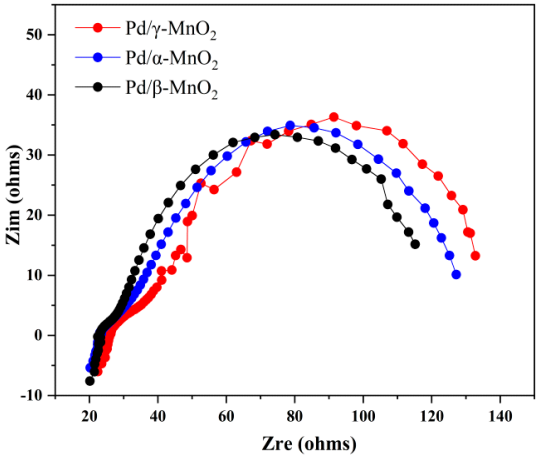

Figure 10. Electrochemical impedance spectra of Pd/α-MnO_2, Pd/β-MnO_2, and Pd/γ-MnO_2 catalysts.

In the preparation of Pd/γ-MnO_2 (see Materials and Methods for details of catalysts preparation), the pH value of the Pd precursor (K_2PdCl_4) solution will also affect the aggregation of Pd nanoparticles. When the pH value of the K_2PdCl_4 was 3, 5, 9, and 11, there is obvious aggregation on the γ-MnO_2, as shown in Figure 11. However, Pd nanoparticles can be homogeneously dispersed on γ-MnO_2 under the condition that the pH value of K_2PdCl_4 is 7. Consequently, the Pd/γ-MnO_2 prepared under the condition that pH = 7 can reach a higher NH_3 yield rate and Faradaic efficiency than that on other catalysts in Figure 12. It also suggests that the aggregation of Pd particles will cause a loss of performance. Figures 11 and 12 suggest that the conditions of strong acidity and alkalinity are unfavorable for Pd^{2+} reduction. This can be recognized as important inspiration in the design of catalysts of electrochemical synthesis of ammonia. The conditions in the catalyst preparation process, such as heating temperature and stirring time, may have a great influence on the catalytic performance and microstructure of the catalysts.

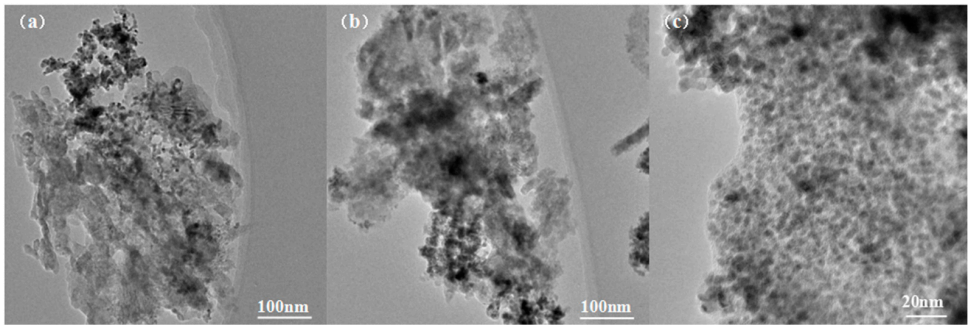

Figure 11. *Cont.*

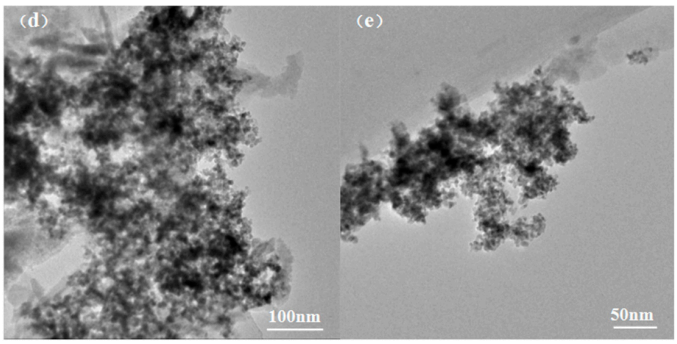

Figure 11. TEM images of Pd/γ-MnO_2 catalysts prepared under different pH value. (**a**) pH = 3; (**b**) pH = 5; (**c**) pH = 7; (**d**) pH = 9; and (**e**) pH = 11.

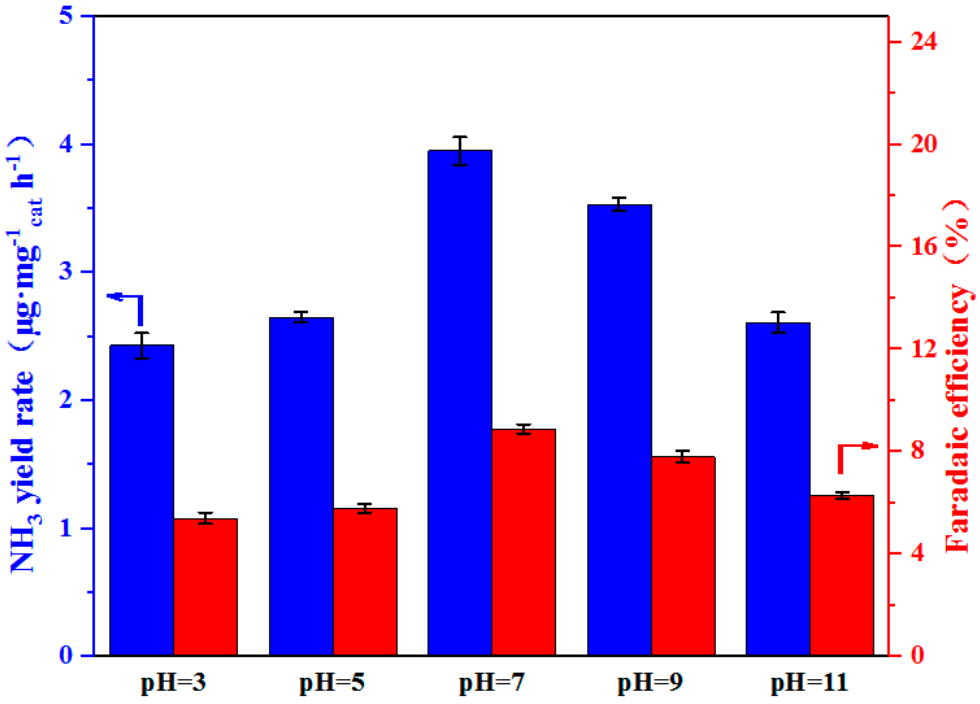

Figure 12. Ammonia synthesis rates and Faradaic efficiencies of Pd/γ-MnO_2 prepared under different pH conditions.

Moreover, we have tested the N source of the produced ammonia. First, we performed control experiments with Ar-saturated electrolyte or without Pd/γ-MnO_2 catalyst. As shown in Figure 13, no apparent NH_3 was detected when the bubbled N_2 gas was replaced by Ar or when a carbon paper electrode without the Pd/γ-MnO_2 catalyst was used. And the 0.1 M KOH without electrodes cannot detect ammonia as well. It suggests that the NH_3 was produced by N_2 reduction in the presence of Pd/γ-MnO_2 catalyst.

The stability of the Pd/γ-MnO_2 catalyst for electroreduction of N_2 to NH_3 was evaluated by consecutive recycling electrolysis. As shown in Figure 14a, only a slight decline in the total current was observed. However, Figure 14b shows that the NH_3 yield rate and Faradaic efficiency decreased to 2.45 μg·mg^{-1}_{cat} h^{-1} (12.25 μg·mg^{-1}_{Pd} h^{-1}) and 5.2%, indicating a loss of electrochemical activity by 40% after the 12 h operation. This loss in the electrochemical activity and selectivity is due to the loss of active Pd surface area caused by the aggregation of Pd nanoparticles on the surface of Pd/γ-MnO_2, as evidenced by TEM images of the Pd/γ-MnO_2 catalyst before and after stability test (Figure 15).

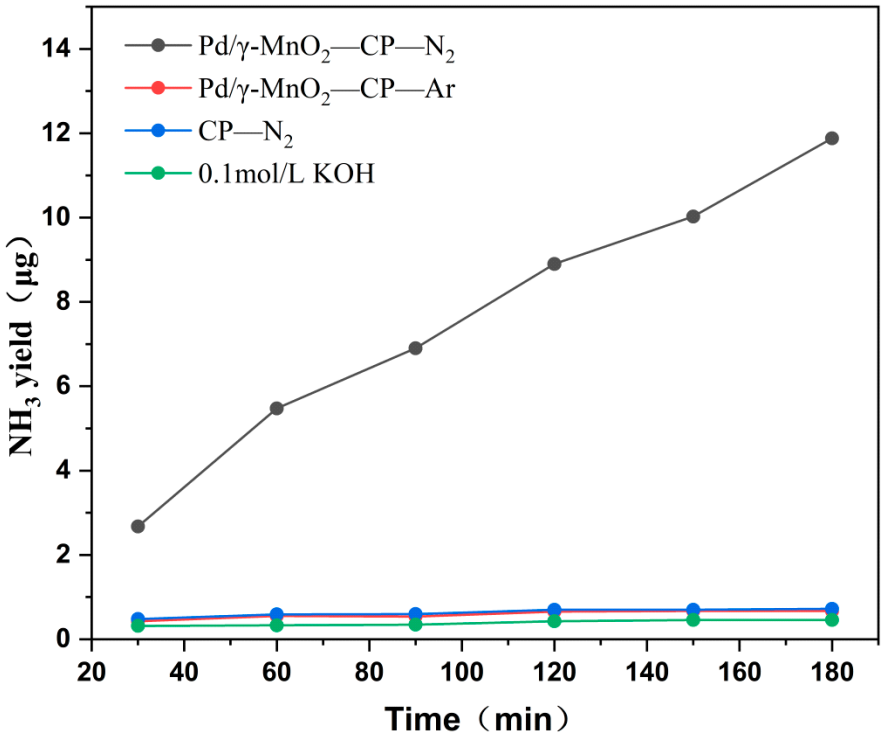

Figure 13. The curve of ammonia yield and time under four different conditions.

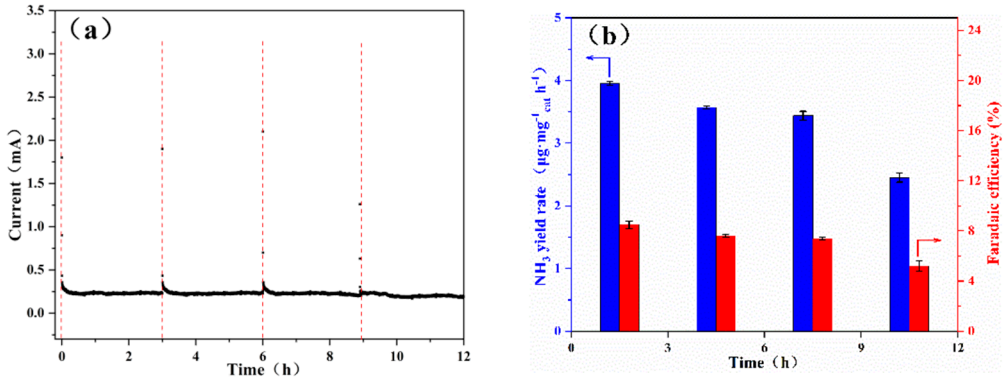

Figure 14. (**a**) Variation of electric current in the four successive operations each lasting 3 h. (**b**) Ammonia synthesis rates and Faradaic efficiency of each electrolysis cycle.

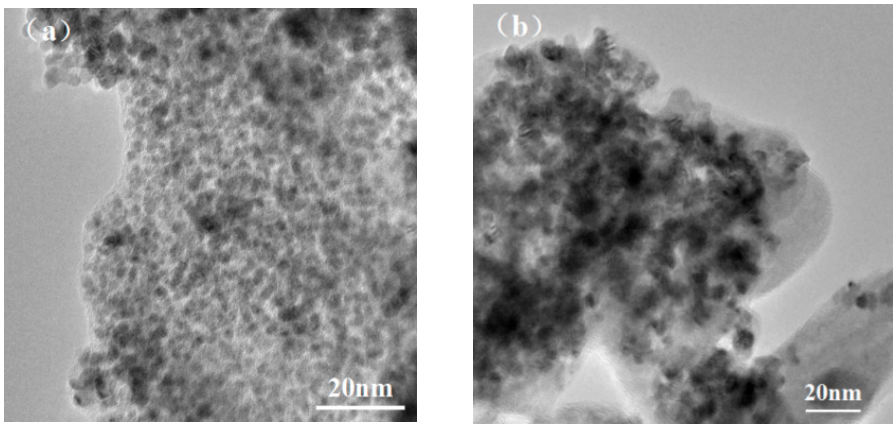

Figure 15. TEM images of the Pd/γ-MnO_2 catalyst before (**a**) and after (**b**) stability test.

3. Materials and Methods

3.1. Materials

Potassium hydroxide and ethylene glycol were obtained from Tianjin Kemiou Chemical Reagent Company (Tianjin, China). Salicylic acid and ammonium sulfate were supplied by Tianjin Seans Biochemical Technology Company (Tianjin, China). N_2 and Ar were supplied by Tianjin Dongxiang Special Gas Company (Tianjin, China). Palladium dichloride was obtained from Ailan (Shanghai) Chemical Technology (Shanghai, China). Sodium borohydride, isopropanol and concentrated sulfuric acid were obtained from Tianjin Jiangtian Chemical Technology (Tianjin, China). Sodium hydroxide was supplied by Tianjin Guangfu Technology Development Company (Tianjin, China).

3.2. Catalyst Preparation

3.2.1. α-MnO_2

First, 1 g of $KMnO_4$ and 0.5 g of $MnCl_2{\cdot}4H_2O$ were dissolved in 140 mL of water, followed by sonication for 30 min. Then the solution was poured into a 200 mL PTFE-lined hydrothermal reactor and reacted for 12 h at 180 °C. The mixture was filtered with suction and rinsed with deionized water after the reaction. The resulting α-MnO_2 was dried at 60 °C overnight.

3.2.2. β-MnO_2

First, 0.632 g of $KMnO_4$ was dissolved in 112 mL of water, and 11 mL of concentrated hydrochloric acid (12 mol/L) was added dropwise with stirring, followed by sonication for 3 h. Then the solution was poured into a 200 mL PTFE-lined hydrothermal reactor and reacted for 12 h at 160 °C. The mixture was filtered with suction and rinsed with deionized water after the reaction. The resulting β-MnO_2 was dried at 60 °C overnight.

3.2.3. γ-MnO_2

0.92 g $(NH_4)S_2O_8$ and 0.4 g $MnCl_2{\cdot}4H_2O$ were dissolved in 60 mL of water respectively and recorded as solution A and solution B. Next, solution B was added dropwise to solution A with stirring. Then the solution was poured into a 200 mL PTFE-lined hydrothermal reactor and reacted for 24 h at 90 °C. The mixture was filtered with suction and rinsed with deionized water after the reaction. The resulting γ-MnO_2 was dried at 60 °C overnight.

3.2.4. Pd/γ-MnO_2

We use polyol reduction method to prepare the Pd/γ-MnO_2 catalyst. First, K_2PdCl_4 (the Pd precursor solution) was prepared by dissolving palladium dichloride in water with KCl. And 120 mg of γ-MnO_2 was dispersed in 120 mL of ethylene glycol, followed by sonication for 1 h. Then, 5 mL of K_2PdCl_4 solution (containing Pd 6 mg/mL) was added into this mixture. After stirring for 30 min at room temperature, the mixture was heated at 130 °C for 2 h. The mixture was filtered with suction and rinsed with deionized water. Then we dried the product at 60 °C for 12 h, with a Pd loading of 20 wt.%. Pd/C, Pd/α-MnO_2, and Pd/β-MnO_2 catalysts with a Pd loading of 20 wt.% were synthesized by the same procedure, except with different carriers.

3.3. Preparations of the Working Electrodes

First, 2 mg of γ-MnO_2-supported Pd nanoparticles catalyst was dispersed in diluted Nafion alcohol solution containing 1 mL ethanol and 45 μL Nafion, which formed a homogeneous suspension after sonication for 2 h. The carbon-paper electrodes were prepared by drop-casting the suspension on carbon paper (1.25×0.8 cm^2), with a total mass loading of 1 mg (of which 20 wt.% is Pd).

3.4. Ammonia Quantification

In this study, NH_3 was quantitatively determined by indophenol blue method. Each sample solution was added with 0.5 mL of 5% salicylic acid solution, 0.1 mL of 1% sodium nitroprusside solution, and 0.1 mL of 0.05 mol/L NaClO solution. Leave at room temperature for 1 h in the dark. Then measure its absorbance by ultraviolet spectrophotometer, contrast with the calibration curve.

3.5. Calculation of the NH_3 Yield Rate the Faradaic Efficiency

NH_3 yield rate the Faradaic efficiency were calculated as follows:

$$\text{Faradaic efficiency} = (3F \times c_{NH_3} \times V)/Q$$

$$\text{Yield rate} = (17c_{NH_3} \times V/(t \times m)$$

F is the Faraday constant (96485 C·mol^{-1}); c_{NH_3} is the concentration of NH_3; V is the volume of the electrolyte; Q is the charge flowed through the electrode; t is the reaction time; and m is the mass of the whole catalyst or precious metal.

4. Conclusions

In this article, we use polyol reduction method to prepare the γ-MnO_2-supported Pd nanoparticles catalyst (Pd/γ-MnO_2), which exhibits effective catalytic activity for the electrochemical ammonia synthesis. The NH_3 yield rate and Faradaic efficiency of Pd/γ-MnO_2 catalyst reaches a maximum value of 19.72 μg·mg$^{-1}{}_{Pd}$ h^{-1} (6.44×10^{-11} mol·s^{-1} cm^{-2}) and 8.4%, respectively, at −0.05 vs. RHE, indicating a synergistic catalytic effect between Pd and Mn. Pd/γ-MnO_2 outperforms other catalysts including Pd/C and γ-MnO_2 because of its synergistic catalytic effect. Moreover, our result shows that γ-MnO_2 is the optimal carrier for Pd nanoparticles among three different crystal forms of MnO_2. Further improvement in research of the interaction between Pd and Mn will be beneficial for the NRR activity and selectivity of the catalyst.

Author Contributions: Conceptualization, methodology, Y.W. and C.S.; formal analysis, validation, and review, Y.W., C.S., and supervision, project management, Y.W., Y.M.; Experimental work and draft writing, C.S. All authors have read and agreed to the published version of the manuscript.

Funding: This research received no external funding.

Acknowledgments: This work has been supervised and reviewed by Luofu Min and Lu Liu.

Conflicts of Interest: The authors declare no conflict of interest.

References

1. Chen, J.G.; Crooks, R.M.; Seefeldt, L.C.; Bren, K.L.; Bullock, R.M.; Darensbourg, M.Y.; Holland, P.L.; Hoffman, B.; Janik, M.J.; Jones, A.K.; et al. Beyond fossil fuel-driven nitrogen transformations. *Science* **2018**, *360*, 873. [CrossRef] [PubMed]
2. Klerke, A.; Christensen, C.H.; Norskov, J.K.; Vegge, T. Ammonia for hydrogen storage: Challenges and opportunities. *J. Mater. Chem. A* **2008**, *18*, 2304–2310. [CrossRef]
3. Zamfirescu, C.; Dincer, I. Using ammonia as a sustainable fuel. *J. Power Sources* **2008**, *185*, 459–465. [CrossRef]
4. Furuya, N.; Yoshiba, H. Electroreduction of nitrogen to ammonia on gas-diffusion electrodes modified by Fe-phthalocyanine. *J. Electroanal. Chem.* **1989**, *263*, 171–174. [CrossRef]
5. Furuya, N.; Yoshiba, H. Electroreduction of nitrogen to ammonia on gas-diffusion electrodes loaded with inorganic catalyst. *J. Electroanal. Chem.* **1990**, *291*, 269–272. [CrossRef]
6. Kordali, V.; Kyriacou, G.; Lambrou, C. Electrochemical synthesis of ammonia at atmospheric pressure and low temperature in a solid polymer electrolyte cell. *Chem. Commun.* **2000**, *48*, 1673–1674. [CrossRef]
7. Kitano, M.; Inoue, Y.; Yamazaki, Y.; Hayashi, F.; Kanbara, S.; Matsuishi, S.; Yokoyama, T.; Kim, S.W.; Hara, M.; Hosono, H. Ammonia synthesis using a stable electride as an electron donor and reversible hydrogen store. *Nat. Chem.* **2012**, *4*, 934–940. [CrossRef]

8. Service, R.F. New recipe produces ammonia from air, water, and sunlight. *Science* **2014**, *345*, 610. [CrossRef] [PubMed]
9. Van der Ham, C.J.M.; Koper, M.T.M.; Hetterscheid, D.G.H. Challenges in reduction of dinitrogen by proton and electron transfer. *Chem. Soc. Rev.* **2014**, *43*, 5183–5191. [CrossRef] [PubMed]
10. Ali, M.; Zhou, F.; Chen, K.; Kotzur, C.; Xiao, C.; Bourgeois, L.; Zhang, X.; MacFarlane, D.R. Nanostructured photoelectrochemical solar cell for nitrogen reduction using plasmon-enhanced black silicon. *Nat. Commun.* **2016**, *7*, 11335. [CrossRef] [PubMed]
11. Brown, K.A.; Harris, D.F.; Wilker, M.B.; Rasmussen, A.; Khadka, N.; Hamby, H.; Keable, S.; Dukovic, G.; Peters, J.W.; Seefeldt, L.C.; et al. Light-driven dinitrogen reduction catalyzed by a CdS: Nitrogenase MoFe protein biohybrid. *Science* **2016**, *352*, 448–450. [CrossRef] [PubMed]
12. Renner, J.N.; Greenlee, L.F.; Herring, A.M.; Ayers, K.E. Electrochemical synthesis of ammonia: A low pressure, low temperature approach. *Electrochem. Soc. Interface* **2015**, *24*, 51–57. [CrossRef]
13. Kyriakou, V.; Garagounis, I.; Vasileiou, E.; Vourros, A.; Stoukides, M. Progress in the electrochemical synthesis of ammonia. *Catal. Today* **2017**, *286*, 2–13. [CrossRef]
14. Shipman, M.A.; Symes, M.D. Recent progress towards the electrosynthesis of ammonia from sustainable resources. *Catal. Today* **2017**, *286*, 57–68. [CrossRef]
15. Soloveichik, G.L. Liquid fuel cells. *Beilstein J. Nanotechnol.* **2014**, *5*, 1399–1418. [CrossRef]
16. Sheets, B.L.; Botte, G.G. Electrochemical nitrogen reduction to ammonia under mild conditions enabled by a polymer gel electrolyte. *Chem. Commun.* **2018**, *54*, 4250–4253. [CrossRef]
17. Bao, D.; Zhang, Q.; Meng, F.L.; Zhong, H.X.; Shi, M.M.; Zhang, Y.; Yan, J.M.; Jiang, Q.; Zhang, X.B. Electrochemical reduction of N_2 under ambient conditions for artificial N_2 fixation and renewable energy storage using N_2/NH_3 cycle. *Adv. Mater.* **2017**, *29*, 1–5. [CrossRef]
18. Wang, Z.; Li, Y.; Yu, H.; Xu, Y.; Xue, H.; Li, X.; Wang, H.; Wang, L. Ambient electrochemical synthesis of ammonia from nitrogen and water catalyzed by flower-like gold microstructures. *ChemSusChem* **2018**, *11*, 3480–3485. [CrossRef]
19. Tsuneto, A.; Kudo, A.; ChemInform, T.S.J. Lithium-Mediated Electrochemical reduction of high Pressure N_2 to NH_3. *J. Electroanal. Chem.* **1994**, *367*, 183–188. [CrossRef]
20. Nash, J.; Yang, X.; Anibal, J.; Wang, J.; Yan, Y.; Xu, B. Electrochemical nitrogen reduction reaction on noble metal catalysts in proton and hydroxide exchange membrane electrolyzers. *J. Electroanal. Chem.* **2017**, *164*, F1712–F1716. [CrossRef]
21. Wang, J.; Yu, L.; Hu, L.; Chen, G.; Xin, H.; Feng, X. Ambient ammonia synthesis via palladium-catalyzed electrohydrogenation of dinitrogen at low overpotential. *Nat. Commun.* **2018**, *9*, 1–7. [CrossRef]
22. Cui, X.; Tang, C.; Zhang, Q. A review of electrocatalytic reduction of dinitrogen to ammonia under ambient conditions. *Adv. Energy Mater.* **2018**, *8*, 1–25. [CrossRef]
23. Lan, R.; Tao, S. Electrochemical synthesis of ammonia directly from air and water using a $Li^+/H^+/NH4^+$ mixed conducting electrolyte. *RSC Adv.* **2013**, *3*, 18016–18021. [CrossRef]
24. Lan, R.; Irvine, J.T.S.; Tao, S. Synthesis of ammonia directly from air and water at ambient temperature and pressure. *Sci. Rep.* **2013**, *3*, 1–7. [CrossRef] [PubMed]
25. Yang, D.; Chen, T.; Wang, Z. Electrochemical reduction of aqueous nitrogen (N_2) at a low overpotential on (110)-oriented Mo nanofilm. *J. Mater. Chem. A* **2017**, *5*, 18967–18971. [CrossRef]
26. Ren, X.; Zhao, J.; Wei, Q.; Ma, Y.; Guo, H.; Liu, Q.; Wang, Y.; Cui, G.; Asiri, A.M.; Li, B.; et al. High-performance N_2 to NH_3 conversion electrocatalyzed by Mo_2C nanorod. *ACS Cent. Sci.* **2019**, *5*, 116–121. [CrossRef] [PubMed]
27. Li, X.; Li, T.; Ma, Y.; Wei, Q.; Qiu, W.; Guo, H.; Shi, X.; Zhang, P.; Asiri, A.M.; Chen, L.; et al. Boosted electrocatalytic N_2 reduction to NH_3 by defect-rich MoS_2 nanoflower. *Adv. Energy Mater.* **2018**, *8*, 1–8. [CrossRef]
28. Zhang, L.; Xie, X.-Y.; Wang, H.; Ji, L.; Zhang, Y.; Chen, H.; Li, T.; Luo, Y.; Cui, G.; Sun, X. Boosting electrocatalytic N_2 reduction by MnO_2 with oxygen vacancies. *Chem. Commun.* **2019**, *55*, 4627–4630. [CrossRef]
29. Wang, Z.; Gong, F.; Zhang, L.; Wang, R.; Ji, L.; Liu, Q.; Luo, Y.; Guo, H.; Li, Y.; Gao, P.; et al. Electrocatalytic hydrogenation of N_2 to NH_3 by MnO: Experimental and theoretical investigations. *Adv. Sci.* **2019**, *6*, 1–8. [CrossRef]
30. Foster, S.L.; Bakovic, S.I.P.; Duda, R.D.; Maheshwari, S.; Greenlee, L.F. Catalysts for nitrogen reduction to ammonia. *Nat. Catal.* **2018**, *1*, 490–500. [CrossRef]

31. Shi, M.M.; Bao, D.; Wulan, B.R.; Li, Y.H.; Zhang, Y.F.; Yan, J.M.; Jiang, Q. Au sub-nanoclusters on TiO_2 toward highly efficient and selective electrocatalyst for N_2 conversion to NH_3 at ambient conditions. *Adv. Mater.* **2017**, *29*, 1–6. [CrossRef] [PubMed]
32. Li, S.J.; Bao, D.; Shi, M.M.; Wulan, B.R.; Yan, J.-M.; Jiang, Q. Amorphizing of Au nanoparticles by CeO_x-RGO hybrid support towards highly efficient electrocatalyst for N_2 reduction under ambient conditions. *Adv. Mater.* **2017**, *29*, 1–6.
33. Ma, J.L.; Bao, D.; Shi, M.M.; Yan, J.M.; Zhang, X.B. Reversible nitrogen fixation based on a rechargeable lithium-nitrogen battery for energy storage. *Chem* **2017**, *2*, 525–532. [CrossRef]
34. McEnaney, J.M.; Singh, A.R.; Schwalbe, J.A.; Kibsgaard, J.; Lin, J.C.; Cargnello, M.; Jaramillo, T.F.; Norskov, J.K. Ammonia synthesis from N_2 and H_2O using a lithium cycling electrification strategy at atmospheric pressure. *Energy Environ. Sci.* **2017**, *10*, 1621–1630. [CrossRef]
35. Chen, G.F.; Cao, X.; Wu, S.; Zeng, X.; Ding, L.X.; Zhu, M.; Wang, H. Ammonia electrosynthesis with high selectivity under ambient conditions via a Li^+ incorporation strategy. *J. Am. Chem. Soc.* **2017**, *139*, 9771–9774. [CrossRef]
36. Giddey, S.; Badwal, S.P.S.; Kulkarni, A. Review of electrochemical ammonia production technologies and materials. *Int. J. Hydrog. Energy* **2013**, *38*, 14576–14594. [CrossRef]
37. Kim, K.; Lee, N.; Yoo, C.Y.; Kim, J.N.; Yoon, H.C.; Han, J.I. Communication-electrochemical reduction of nitrogen to ammonia in 2-Propanol under ambient temperature and pressure. *J. Electrochem. Soc.* **2016**, *163*, F610–F612. [CrossRef]
38. Chen, S.; Perathoner, S.; Ampelli, C.; Mebrahtu, C.; Su, D.; Centi, G. Electrocatalytic synthesis of ammonia at room temperature and atmospheric pressure from water and nitrogen on a carbon-nanotube-based electrocatalyst. *Angew. Chem. Int. Ed.* **2017**, *56*, 2699–2703. [CrossRef]
39. Liu, Y.; Huang, B.M.; Chen, X.F.; Tian, Z.Q.; Zhang, X.Y.; Tsiakaras, P.; Shen, P.K. Electrocatalytic production of ammonia: Biomimetic electrode-electrolyte design for efficient electrocatalytic nitrogen fixation under ambient conditions. *Appl. Catal. B* **2020**, *271*, 1–10. [CrossRef]
40. Ramaiyan, K.P.; Ozden, S.; Maurya, S.; Kelly, D.; Babu, S.K.; Benavidez, A.; Garzon, F.G.; Kim, Y.S.; Kreller, C.R.; Mukundan, R. Molybdenum carbide electrocatalysts for electrochemical synthesis of ammonia from nitrogen: Activity and stability. *J. Electrochem. Soc.* **2020**, *167*, 1–10. [CrossRef]
41. Skulason, E.; Bligaard, T.; Gudmundsdottir, S.; Studt, F.; Rossmeisl, J.; Abild-Pedersen, F.; Vegge, T.; Jonsson, H.; Norskov, J.K. A theoretical evaluation of possible transition metal electro-catalysts for N_2 reduction. *Phys. Chem. Chem. Phys.* **2012**, *14*, 1235–1245. [CrossRef]
42. Vojvodic, A.; Medford, A.J.; Studt, F.; Abild-Pedersen, F.; Khan, T.S.; Bligaard, T.; Norskov, J.K. Exploring the limits: A low-pressure, low-temperature Haber-Bosch process. *Chem. Phys. Lett.* **2014**, *598*, 108–112. [CrossRef]
43. Vojvodic, A.; Norskov, J.K. New design paradigm for heterogeneous catalysts. *Natl. Sci. Rev.* **2015**, *2*, 140–143. [CrossRef]
44. Wickman, B. Depth probing of the hydride formation process in thin Pd films by combined electrochemistry and fiber optics-based in situ UV/vis spectroscopy. *Phys. Chem. Chem. Phys.* **2015**, *17*, 18953–18960. [CrossRef]
45. Hara, M.; Linke, U.; Wandlowski, T. Preparation and electrochemical characterization of palladiumsingle crystal electrodes in 0.1 M H_2SO_4 and $HClO_4$ part I. low-index phases. *Electrochim. Acta* **2007**, *52*, 5733–5748. [CrossRef]
46. Gao, D.; Zhou, H.; Cai, F.; Wang, D.; Hu, Y.; Jiang, B.; Cai, W.B.; Chen, X.; Si, R.; Yang, F.; et al. Switchable CO_2 electroreduction via engineering active phases of Pd nanoparticles. *Nano Res.* **2017**, *10*, 2181–2191. [CrossRef]